Lattice Dynamics of Dense Lithium

F. A. Gorelli,[1,2] S. F. Elatresh,[3] C. L. Guillaume,[4] M. Marqués,[4,‡] G. J. Ackland,[4] M. Santoro,[1,5] S. A. Bonev,[3,6,*] and E. Gregoryanz[4,†]

[1]*LENS, European Laboratory for Non-Linear Spectroscopy, University of Florence, I-50121 Florence, Italy*
[2]*IPCF-CNR, UOS Roma, Piazzale Aldo Moro 5, 00185 Roma, Italy*
[3]*Department of Physics, Dalhousie University, Halifax, Nova Scotia B3H 3J5, Canada*
[4]*SUPA, School of Physics and Astronomy and Centre for Science at Extreme Conditions, The University of Edinburgh, Edinburgh, EH9 3JZ, United Kingdom*
[5]*IFAC-CNR, Via Madonna del Piano 10, I-50019 Sesto Fiorentino, Italy*
[6]*Lawrence Livermore National Laboratory, Livermore, California 94550, USA*

(Received 14 June 2011; published 30 January 2012)

We report low-frequency high-resolution Raman spectroscopy and *ab-initio* calculations on dense lithium from 40 to 200 GPa at low temperatures. Our experimental results reveal rich first-order Raman activity in the metallic and semiconducting phases of lithium. The computed Raman frequencies are in excellent agreement with the measurements. Free energy calculations provide a quantitative description and physical explanation of the experimental phase diagram only when vibrational effect are correctly treated. The study underlines the importance of zero-point energy in determining the phase stability of compressed lithium.

DOI: 10.1103/PhysRevLett.108.055501 PACS numbers: 63.20.−e, 61.50.Ks, 62.50.−p, 64.60.−i

Despite the huge interest shown by theoretical and experimental physicists ([1–12] and references therein) the self consistent phase diagram of elemental lithium at high pressures eluded its pursuers for a long time. The problems arise because of experimental difficulties associated with Li at high static pressures [13] and the presence of complex structures that can not be easily predicted theoretically or solved crystallographically. Very recently, the phase diagram was mapped up to 130 GPa in a wide temperature range using synchrotron x-ray diffraction techniques, revealing three novel solid phases and a drop of the melting temperatures to below 200 K between 40 and 60 GPa [14]. These structural data paved the way for a combined experimental and theoretical crystallographic solution and a study of electronic properties [15], which in turn reconciled the experimentally observed unusual behavior of resistivity versus pressure in dense Li [10].

While there is an overall good agreement between experimental and theoretical studies regarding the stability of some of the complex solid phases, in particular *oC*24 (*Cmca*) and *oC*40 (*C*2*cb* or *Aba*2), several important questions remain unresolved. For example, theoretical structural searches at 0 K [16] place *oC*40 in the pressure range where *oC*88 is found experimentally at 200 K [14] and although the *oC*88 structure (*C*2*mb* or *Abm*2) was determined [15], it does not have the lowest enthalpy [17] at any pressure. The question of the stability of *oC*88 is related to two broader issues, namely, the importance of phonon lattice dynamics in the high-pressure phase diagram of Li, and the accuracy of *ab-initio* methods used to predict it. Indeed, the light atomic mass of Li, the presence of numerous competitive structures with enthalpies within a few meV, and the large variation in unit cell sizes means that dynamical effects are likely to play an important role. However, previous theoretical studies have been mostly limited to 0 K enthalpy calculations. Experimental vibrational data are also very limited because of the serious technical difficulties associated with containment of Li under static pressure [13,14].

To date there is only one experimental optical spectroscopy study on dense Li [6]. However, the reflectivity measurements and sample photos presented there [6] showed sample darkening starting from about 22 GPa, which is at variance with resistivity measurements [10] that found Li to be still in the metallic fcc phase at this pressure. These observations are consistent with our optical studies in which we observed Li reacting under pressure. We observed sample darkening and the appearance of broad, weak Raman bands identical to those reported in Ref. [6] at moderate pressures whenever the samples have been originally contaminated (compare Fig. 3 in [14] with Figs. 3 and 4 in Ref. [6]). Furthermore, some of the Raman frequencies reported in Ref. [6] are too high for any of the Li structures expected at the measured pressures [18]. Therefore, achieving reliable optical measurements on high-pressure Li remains a challenge and such probes could potentially reveal exciting aspects related to the lattice dynamics of the lightest metal.

In this Letter, we report low-temperature Raman measurements on solid lithium phases from 40 to 200 GPa, by far, the highest pressure at which lithium was studied experimentally. First-order Raman activity is found in all four phases observed in this high-pressure range, starting with a doublet in *cI*16 ($I\bar{4}3d$), very low-frequency modes

in the metallic $oC88$ ($C2mb$) phase, intense and rich spectrum in the semiconducting $oC40$ ($C2cb$) phase, and an intense mode in the $oC24$ ($Cmca$) structure persisting up to 200 GPa. The experimental Raman modes are reproduced very well by *ab-initio* density functional (DFT) calculations. We have then carried out full Brillouin zone (BZ) phonon calculations to obtain Gibbs free energies for selected structures and determined the finite-temperature phase stability of Li up to 200 GPa and 300 K, which is consistent with the experimental measurements.

For full details of the experimental procedures, sample loading and theoretical phonon and enthalpy calculations we refer the reader to the supplementary materials [19] and the Refs. [14,20–27]. Measured Raman spectra are shown in Fig. 1. Between ambient and ~40 GPa, Li adopts the monatomic bcc and fcc [2,14] structures that are not first-order Raman active. We have not attempted any measurements of the $hR1$ phase, which, also being monatomic, is not expected to be Raman active. The $cI16$ phase exhibits a strong doublet and the overall appearance of its spectrum is very similar to the one observed in the $cI16$ phase of Na [22]. We have also conducted several isobaric temperature scans observing gradual broadening of the spectra and their disappearance at temperatures above ~200 K in between 45 and 60 GPa; this corresponds to the previously reported $cI16$ melting temperature [14]. Upon compression, the frequencies of the observed peaks in the $cI16$ phase slowly increase. The picture changes abruptly above ~60 GPa where Li transforms to $oC88$. We observe two relatively weak peaks, which are significantly softer than any of the optical modes in $cI16$. The lowest frequency band at 66 GPa is located at ~35 cm^{-1}; to our knowledge this is the lowest Raman frequency of any material observed at such high pressures. The $oC88$ phase has a narrow pressure stability range, extending up to 70 GPa. Above 70 GPa, Li adopts the semiconducting $oC40$ phase, accompanied by a significant increase of Raman activity and a visible sample darkening. The $oC40$ phase has more than 20 observable Raman bands (Fig. 2), with most frequencies increasing with pressure. However, there is some softening of the lowest frequency mode (see below). In the metallic $oC24$ structure, we observe only one intense mode accompanied by several weak ones which become indistinguishable from the background at high pressures. The strongest mode increases slowly in frequency with pressure, reaching 330 cm^{-1} at 200 GPa (Figs. 1 and 2).

The extremely low (Γ-point) Raman frequencies in $oC88$ can be a result of one or both of the following: (i) its larger unit cell (smaller Brillouin zone) compared to that of the other Li structures, i.e., band folding; and (ii) actually having softer lattice phonon modes. If the latter is true, then $oC88$ might have both lower zero-point energy (ZPE) and higher entropy than the competing phases. This could explain the fact that *ab-initio* calculations excluding these effects did not find $oC88$ to be preferred [16]. Here we observe that the $cI16 \rightarrow oC88$ transition can be induced by increasing T at fixed pressure (Fig. 1), suggesting that entropic effects help to stabilize it at finite temperature. In order to better understand the role of dynamics, we now turn our attention to a theoretical analysis of the lattice phonons.

The computed Γ-point modes are compared with measurements in Fig. 2. We observe almost identical pressure dependence of the modes in the $oC40$ and $oC24$ phases

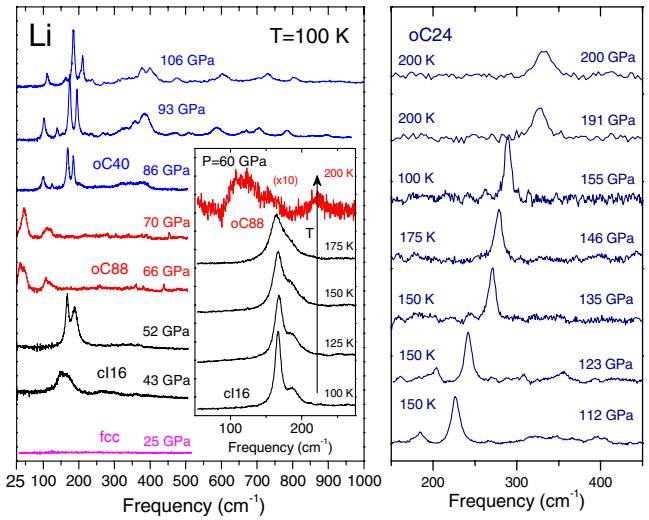

FIG. 1 (color online). Left panel: Representative Raman spectra of the fcc, $cI16$, $oC88$ and $oC40$ phases shown at different pressures at 100 K. Crystal structures are named in the figure and emphasized by color in the online version. Inset, variation of Raman spectrum with heating through the $cI16 \rightarrow oC88$ transition at 60 GPa. Right panel: Representative spectra of the $oC24$ phase at different pressures and temperatures.

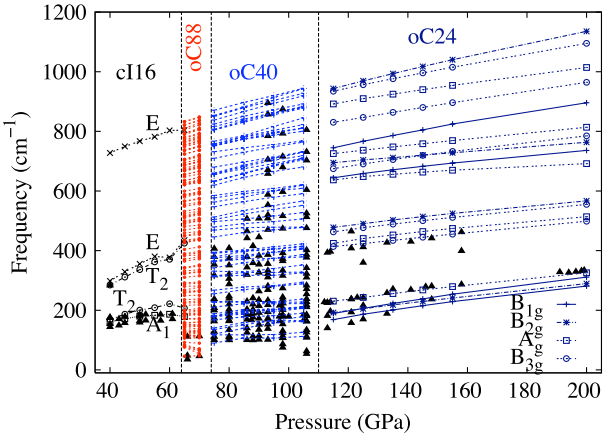

FIG. 2 (color online). The frequencies of the Raman modes of the $cI16$, $oC88$, $oC40$ and $oC24$ phases as a function of pressure at 100 K. Black filled triangles show the experimentally observed frequencies, other open symbols show the calculated ones. Lines are the theoretical Raman modes with symmetry labels for the $cI16$ and $oC24$ structures. Vertical lines indicate phase boundaries, emphasized by color in the online version.

(Fig. 2). The DFT results reproduce the observed Raman peaks very well, except for the one lowest frequency extremely weak mode, experimentally observed between 95 and 106 GPa in $oC40$ (see supplementary materials [19]). Without precise *in situ* x-ray diffraction and optical measurement (currently not available), it is difficult to assign this mode but we note that its frequency seems to lie on the extension of one of $oC88$ modes, far into the stability field of $oC40$. It is also interesting to point out that the $oC24$ phase, which is dynamically unstable below 90 GPa, has modes with positive frequencies close to those observed in the experiments at around 106 GPa (see also below).

The phonon contributions to the Helmholtz free energies (F_{ph}) for the relevant Li phases are plotted as a function of pressure in Figs. 3(a) and 3(b). The ZPE's are sufficiently large that even small relative variations can affect the predicted stability. If expressed in Kelvin, a ZPE of 75 meV corresponds to $T = 870$ K, which is significantly larger than the melting temperature of Li at around 50 GPa, where it is only ~200 K. Therefore, Li is very much a quantum solid below its melting curve up to at least 120 GPa. However, determining to what degree the quantum ion dynamics is responsible for the extremely low melting T of Li requires careful evaluation of classical and quantum free energies of both solid and liquid Li near the melting curve; zero-point energy effects will be significant in the liquid as well, and may cancel out most of the solid phase quantum corrections. Furthermore, we note that the slope of F_{ph} vs P for $cI16$ changes at about 50 GPa, in the region of the melting curve minimum. This effect is due to softening of the acoustic modes of $cI16$, and a rapid change of the internal parameter up to the special value $x = \frac{1}{8}$. Such large changes in structure within a symmetry group are typically due to changes in the bonding character, towards an electride structure as was observed in potassium [28]. The Debye temperature of $cI16$ would show a correlation (inverse) with the changes in melting T, although the ZPE increases monotonically with P.

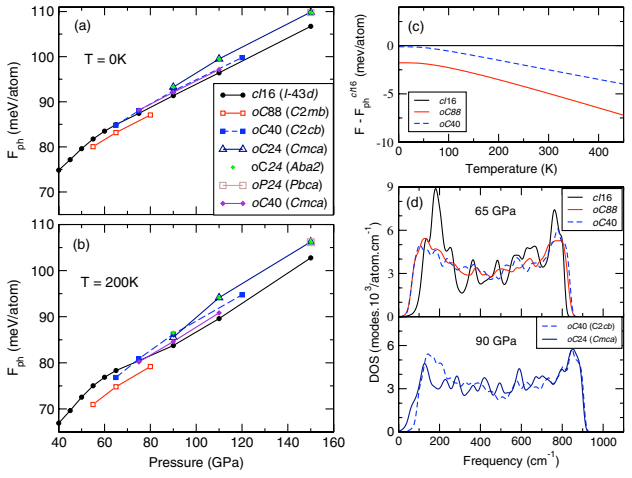

FIG. 3 (color online). Vibrational free energies, F_{ph} (the final term in Eq. (1)), of Li structures at (a) 0 K and (b) 200 K. (c) Temperature dependence at 65 GPa of the relative F_{ph}'s of the three lowest-enthalpy structures at this pressure. (d) Phonon density of states of selected Li structures at 65 GPa (upper panel) and 90 GPa (lower panel).

The $oC88$ phase stands out in having a distinctly lower F_{ph} between 55 and 80 GPa than the other structures. The effect is enhanced with T, meaning that the entropy plays a significant role. The temperature dependence of the relative Helmholtz energies of $oC88$, $oC40$ and $cI16$ at 65 GPa are shown in Fig. 3(c). By 200 K, most of the difference between $cI16$ and the other two comes from the entropy rather than ZPE. Phonon densities of states (DOS) of selected structures at 65 and 90 GPa are shown in Fig. 3(d). Despite the large variations in unit cell sizes, the phonon bandwidths of all structures are nearly the same. Compared to $cI16$, the larger unit cells have modes with slightly higher frequencies and also more phonon states with low frequencies. The latter is a combination of both optical and acoustic modes, which are responsible for their larger entropy. The extra DOS below 100 cm^{-1} seen in *Cmca*-24 come from optical modes; however, they are not sufficient to change its relative free energy significantly. To determine the thermodynamic stability of the various phases at 0 and finite T, we have calculated their relative Gibbs free energies, using the harmonic approximation:

$$G = U + PV + kT \int \ln[2\sinh(\hbar\omega/2kT)]g(\omega)d\omega. \quad (1)$$

Here U and P are the DFT total energy and external pressure of the static structures and $g(\omega)$ is the calculated phonon DOS at frequency ω. Inclusion of phonon pressures (on the order of 1–2 GPa) was determined to not alter relative stabilities. The Gibbs free energies of each structure are calculated only for pressures where the given structure is dynamically stable. The computed Gibbs free energies are shown in Fig. 4. As in the previous *ab-initio* study [15], the $oC88$ phase is not stable at any pressures based on static DFT enthalpy alone. The effect of ZPE is shown in Fig. 4(b), the Gibbs free energy of $oC88$ becomes just about equal to that of $cI16$ near 65 GPa; the differences are too small to allow us to conclude which structure is preferred. At finite T, however, $oC88$ becomes stable and its stability range increases with T in excellent agreement with the experimental measurements. It is worth noting, that the theoretical structural search study, which predicted $oC56$ but did not find $oC88$, did not include the effects of lattice vibrations in the calculations [16]. Our own calculations of $oC56$ (see supplementary materials [19]) find that including phonons, and PBE exchange correlation in place of LDA, raises the predicted transition pressure by some 50 GPa, to beyond the range accessed in the experiment and therefore consistent with our observation of stable $oC24$ up to 200 GPa. Interestingly, in the region (100 GPa–150 K)

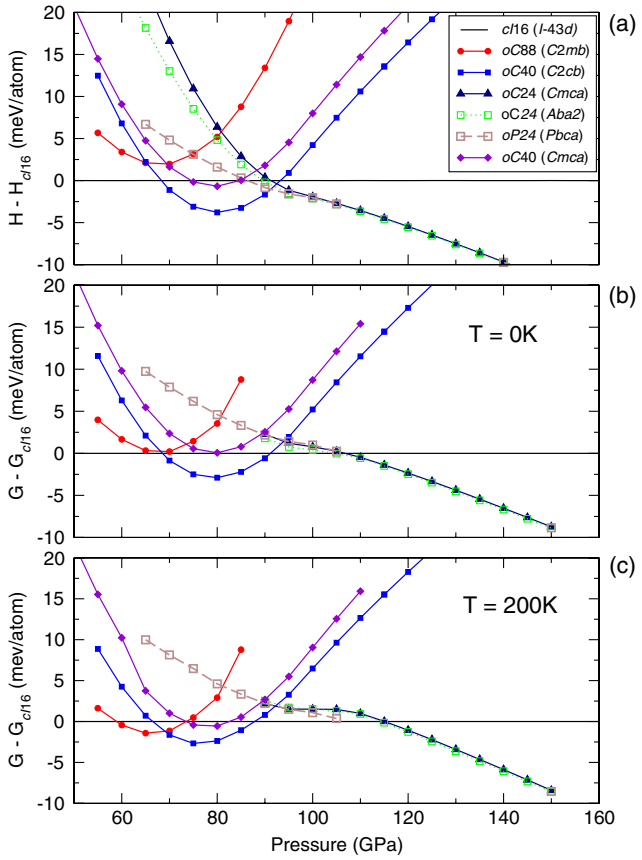

FIG. 4 (color online). Relative to $cI16$ free energies of selected Li structures (a) neglecting ZPE at 0 K [17], $H = U + PV$, (b) with ZPE at 0 K, and (c) at 200 K.

where experimentally we observe the low-frequency mode in $oC40$ (see above), we find that the $cI16$ structure is preferred over both $oC40$ and $Cmca$-24 by about 2 meV. This anomaly might be connected to the soft mode reported here but other possible explanation could include such effects as a larger potential barrier associated with the $oC40 \rightarrow cI16$ than the $oC40 \rightarrow oC24$ transition and/or nonhydrostatic effects which would be non-negligible at 100 GPa and below 200 K (see supplementary materials [19]).

To summarize, we have performed the first series of accurate Raman frequency measurements on dense lithium, backed with electronic structure calculations which enable us to identify the observed modes and calculate finite-temperature thermodynamic properties. The inclusion of phonon free energies resolves the problem of the thermodynamic stability of $oC88$. The work underlines the importance of considering lattice dynamics for structural studies at high pressure, even for systems which are not usually considered as quantum solids at ambient conditions.

We acknowledge the support from the U. K. Engineering and Physical Sciences Research Council; the EU Contract No. FP7 G. A. No 228334 laserlabeurope, and the Ente Cassa di Risparmio di Firenze supporting research at LENS under the grant ''Firenze Hydrolab''; financial support from a Clarín fellowship (FICYT) and the Spanish MALTA Consolider Project; and support by Acenet, CFI, and LLNL for computational resources. Work at LLNL was prepared under Contract DE-AC52-07NA27344.

*stanimir.bonev@dal.ca
bonev@llnl.gov
†e.gregoryanz@ed.ac.uk
‡Present address: Departamento de Química Física y Analítica, Universidad de Oviedo, E-33006 Oviedo, Spain.

[1] J. B. Neaton and N. W. Ashcroft, Nature (London) **400**, 141 (1999).
[2] M. Hanfland, K. Syassen, N. Christensen, and D. Novikov, Nature (London) **408**, 174 (2000).
[3] K. Shimizu, H. Ishikawa, D. Takao, T. Yagi, and K. Amaya, Nature (London) **419**, 597 (2002); V. Struzhkin, M. Eremets, W. Gan, H. K. Mao, and R. Hemley, Science **298**, 1213 (2002); S. Deemyad and J. S. Schilling, Phys. Rev. Lett. **91**, 167001 (2003).
[4] G. Ackland and I. MacLeod, New J. Phys. **6**, 138 (2004).
[5] R. Rousseau, K. Uehara, D. Klug, and J. Tse, Chem. Phys. Chem. **6**, 1703 (2005).
[6] A. F. Goncharov, V. V. Struzhkin, H. K. Mao, and R. J. Hemley, Phys. Rev. B **71**, 184114 (2005).
[7] I. Tamblyn, J. Y. Raty, and S. A. Bonev, Phys. Rev. Lett. **101**, 075703 (2008).
[8] C. J. Pickard and R. J. Needs, Phys. Rev. Lett. **102**, 146401 (2009).
[9] Y. Yao, J. S. Tse, and D. D. Klug, Phys. Rev. Lett. **102**, 115503 (2009).
[10] T. Matsuoka and K. Shimuzu, Nature (London) **458**, 186 (2009).
[11] A. Lazicki, Y. Fei, and R. Hemley, Solid State Commun. **150**, 625 (2010).
[12] E. R. Hernández, A. Rodriguez-Prieto, A. Bergara, and D. Alfé, Phys. Rev. Lett. **104**, 185701 (2010).
[13] M. Hanfland, I. Loa, K. Syassenb, U. Schwarzc, K. Takemura, Solid State Commun. **112**, 123 (1999).
[14] C. L. Guillaume, E. Gregoryanz, O. Degtyareva, M. McMahon, M. Hanfland, S. Evans, M. Guthrie, S. Sinogeikin, and H-K. Mao, Nature Phys. **7**, 211 (2011).
[15] M. Marqués, M. McMahon, E. Gregoryanz, M. Hanfland, C. L. Guillaume, C. J. Pickard, G. J. Ackland, and R. J. Nelmes, Phys. Rev. Lett. **106**, 095502 (2011).
[16] J. Lv, Y. Wang, L. Zhu, and Y. Ma, Phys. Rev. Lett. **106**, 015503 (2011).
[17] In this Letter we use the term *enthalpy* to refer to the calculated total energy from DFT plus PV, excluding any zero-point or vibrational energy.
[18] J. S. Tse, D. D. Klug, and T. Iitaka, Phys. Rev. B **73**, 212301 (2006).
[19] See Supplemental Material at http://link.aps.org/supplemental/10.1103/PhysRevLett.108.055501 for experimental and theoretical details, our calculations on the $oC56$ structure and the stability of the $cI16$ phase.

[20] M. McMahon *et al.*, Proc. Natl. Acad. Sci. U.S.A. **104**, 17 297 (2007).
[21] E. Gregoryanz, L. Lundegaard, M. McMahon, C. Guillaume, R. Nelmes, and M. Mezouar, Science **320**, 1054 (2008).
[22] M. Marqués, M. Santoro, C. L. Guillaume, F. Gorelli, J. Contreras-Garcia, R. T. Howie, A. F. Goncharov, and E. Gregoryanz, Phys. Rev. B **83**, 184106 (2011).
[23] P. Giannozzi *et al.*, J. Phys. Condens. Matter **21**, 395502 (2009); see also http://www.quantum-espresso.org.
[24] X. Gonze *et al.*, Comput. Phys. Commun. **180**, 2582 (2009).
[25] C. Hartwigsen, S. Goedecker, and J. Hutter, Phys. Rev. B **58**, 3641 (1998).
[26] M. Krack, Theor. Chem. Acc. **114**, 145 (2005).
[27] X. Gonze, Phys. Rev. B **55**, 10 337 (1997); X. Gonze and C. Lee, *ibid.* **55**, 10 355 (1997).
[28] M. Marqués, G. J. Ackland, L. F. Lundegaard, G. Stinton, R. J. Nelmes, and M. I. McMahon, Phys. Rev. Lett. **103**, 115501 (2009).